Hydrogen isotope permeation through yttria coatings on Eurofer in the diffusion limited regime

J. Engels, A. Houben, and Ch. Linsmeier

Forschungszentrum Jülich GmbH, Institut für Energie- und Klimaforschung – Plasmaphysik, 52425 Jülich, Germany

Abstract

In fusion power plants a tritium permeation barrier is required in order to prevent the loss of the fuel. Moreover, the tritium permeation barrier is necessary to avoid that the radioactive tritium accumulates in the first wall, the cooling system, and other parts of the power plant. Oxide thin films, e.g. Al_2O_3, Er_2O_3 and Y_2O_3, are promising candidates as tritium permeation barrier layers. With regard to the application, this is especially true for yttrium due to its favorably short decay time after neutron activation compared to the other candidates. The Y_2O_3 layers with thicknesses from 100 nm to 500 nm are deposited on both sides of Eurofer substrates by RF magnetron sputter deposition. Some of the samples are additionally deposited with palladium thin films to analyse the limited regime. During the annealing in the experiments the palladium layers do not show any crack formation or delamination, verified by scanning electron microscopy. After annealing the cubic crystal structure of the Y_2O_3 layers is verified by X-ray diffraction. The cubic phase contains a small amount of a monoclinic phase, which is eliminated after the permeation measurements. The permeation reduction factors of the samples are determined in gas-driven deuterium permeation experiments. A permeation reduction of 5000 of the yttria thin film is verified. The diffusion limited regime is identified by the pressure dependence of the permeation measurement and by permeation experiments with the palladium top layers on the Y_2O_3 thin films. Furthermore, the activation energy of the permeation through the yttria thin films is dertermined. Pre-annealing times for more than 70 h of the Y_2O_3 thin films and permeation measurements with temperature cycles for 20 days are performed to show the stability of the permeation flux and hence the microstructure of the barrier layers. Measurement times at each constant temperature level of more than 25 h are required for the stabilization of each permeation flux to a constant value. The permeation measurement setup is enhanced to enable a continuously running equipment for these measurement times.

Keywords:

Deuterium, Tritium permeation barrier, Yttria, Palladium top layers, Diffusion limited regime

1 Introduction

The safe operation with radioactive tritium is one of the main aspects in future fusion power plants. Suppression of tritium permeation through the first wall is required because the structural steel components show high permeability of hydrogen isotopes in the operational temperature range [1, 2, 3]. Moreover, permeation barriers reduce the tritium fuel loss. As a consequence, the Tritium Breeding Ratio (TBR) of the power plant increases. For a viable power plant a sufficient large TBR is required. Therefore, a permeation barrier with a Permeation Reduction Factor (PRF) in the range of 10 to 1000 is necessary [4, 5, 6, 7, 8]. Several thin ceramic coatings, e.g. Al_2O_3, Er_2O_3, and Y_2O_3, fulfill these requirements [9, 10, 11, 12, 13, 14, 15, 16]. Yttria (Y_2O_3) is considered as an ideal candidate for tritium permeation barrier material, due to its favorably low activation behavior [17, 18, 19, 20, 21, 22, 23]. In this work, the tritium permeation is simulated with the hydrogen isotope deuterium. Both hydrogen isotopes show similar permeation characteristics. The different masses of the isotopes $m_{D/T}$ lead to different diffusivities $D_{D/T}$, which for most metals is expressed by $D_T/D_D = \sqrt{m_D/m_T}$ [15]. Thus, the influence of the isotope effect on the permeation reduction is limited. However, there is an ongoing scientific discussion of the isotope effect in the context of the tritium permeation through ceramic coatings, which is beyond the scope of this initial study [24].

Fusion power plants are not the only application for permeation barriers. Hydrogen permeation barriers are also a relevant issue in the development of technologies for the hydrogen economy, since variable gas compositions and operation temperatures pose a challenge to the metallic materials in the systems of the hydrogen technologies in terms of hydrogen embrittlement and surface corrosion. The steel components in systems such as catalytic reactors, fuel cells, and other hydrogen production facilities are in direct contact with the chemically reactive gases [25, 26, 27, 28]. Ceramic thin films as protective and hydrogen permeation barrier coatings reduce corrosion and embrittlement of metallic materials. This application for permeation barriers is introduced in [16].

The measurement of the permeation reduction of the barrier material is not sufficient for the prediction of the PRF of the barrier coating in the first wall component in fusion power plants. Another necessary analysis is the identification of the rate-limiting regime of the permeation process, since surface effects might lead to a difference between the permeation reduction measured in laboratory experiments and the actual permeation reduction under operation conditions. This is a relevant issue in the case of the surface limited regime. In this study the limiting regime is analyzed with respect to the pressure dependence on the permeation flux, the thin film thickness dependence, and the permeation measurement through yttria samples with palladium top layers.

One of the candidates for the DEMO first wall components is the Eurofer/yttria/tungsten sandwich structure. Thus, the permeation measurement through the Eurofer/yttria/palladium samples of this study is a first approximation for understanding hydrogen transport in the DEMO (DEMOnstration Power Plant) first wall components. According to the best of the authors' knowledge, there is no previous literature on permeation experiments through yttria samples with this sandwich structure. The yttria and the palladium thin films are deposited on Eurofer substrates. Eurofer is a reduced activation ferritic martenstic steel, developed as a structural material for fusion application [29].

Possible changes in the crystallographic phase can influence the permeation characteristics of the barrier coating on longer time scales. This is important in terms of predicting the PRF for the long term application in a fusion power plants. Therefore, in this study pre-annealing times for more than 70 h at 550 °C are performed. Additionally, the yttria thin films are annealed in several cyclic permeation measurements between 300 °C and 550 °C for 20 days. The crystallographic phase of the yttria films is analyzed before and after the permeation measurement.

Moreover, at each constant temperature level permeation measurements of more than 25 h are performed with continuously running measurement equipment in order to stabilize the permeation flux to a constant value. This long stabilization time of the permeation flux is necessary to investigate the limiting regime with the method of the pressure dependence on the permeation flux.

2 Materials and methods

2.1 Magnetron deposition and annealing

This publication is focused on yttria films that are manufactured by a magnetron sputter process, named "hot metallic mode" in [16]. Although named "hot metallic" the deposited yttria thin film is a ceramic coating. The details of the yttria deposition process parameters are explained in [16, 30] and the sputter mechanisms are discussed in [4].

The yttria thin films are deposited on both sides of mirror polished Eurofer substrates by magnetron sputtering with an RF current source and with the reactive oxygen in the argon plasma. In a single deposition process, several Eurofer substrates with a thickness of 0.3 mm and a diameter of 2.5 cm are placed on the sample stage, which rotates with 20°/s to enhance the homogeneity of the deposited thin film. The yttria thin film thickness is 510 nm at each side of all standard samples with and without the palladium top layers. Only one sample is manufactured with the thinner coating thicknesses of 100 nm at the first side and 260 nm at the second side. It is referred to the "thin sample" in the following.

During the annealing at 550 °C the difference in the thermal expansion coefficients of the Eurofer substrate ($12 \cdot 10^{-6}\,\mathrm{K}^{-1}$ [31]) and the yttria thin film ($8 \cdot 10^{-6}\,\mathrm{K}^{-1}$ [32]) leads to thermal stress and possibly crack formation in the yttria thin films. In order to reduce the surface temperature differences between the deposition process and the subsequent experiments (and therefore the stress induced by the deposition), the substrate surfaces are heated up to 300 ± 50 °C during the magnetron deposition process. The such produced thin films show no crack formation after annealing at 550 °C, as it is illustrated in the SEM images in figure 2 and in [16].

The palladium thin films are deposited in a magnetron process with a DC current source and a plasma power density of 0.8 W/l. The pure palladium target with a purity of 99.95 % (Kurt J. Lesker Company) is sputtered with an argon pressure of $6 \cdot 10^{-3}$ mbar, a deposition voltage of 510 V, and a sample stage rotation of 20 °/s. All palladium thin films are 75 nm thick, which requires a process time of 5 min.

After deposition, the yttria coated samples are annealed at 550 °C for more than 15 h in a vacuum tube furnace at a pressure of $\leq 1 \cdot 10^{-6}$ mbar to achieve the cubic phase structure of the Y_2O_3 system [11]. The Eurofer/yttria/palladium system is manufactured with the sandwich structure of the two deposition processes of both materials and it is pre-annealed for 70 h in the oven and additionally for 7 days in the temperature cycle of a permeation measurement.

2.2 Analysis methods

The microstructures of the surfaces and of the cross sections of the thin film coatings are investigated using a dual beam Focused Ion Beam (FIB) / Scanning Electron Microscope (SEM) device (Carl Zeiss Crossbeam 540), equipped with an energy-dispersive X-ray spectrometer (EDX). FIB/SEM equipment is used for the production of cross-sections for scanning electron microscopy studies.

The crystal structure of the Y_2O_3 films is characterized by means of an X-ray diffractometer (XRD) using Cu-Kα radiation (BRUKER D8 Discover). The diffraction pattern (Bragg-Brentao geometry) is recorded in a 2Θ angle range of 16° to 68° with 0.02°/step.

2.3 Permeation measurement procedure

The permeation setup is described in detail in [17, 4]. In the measurement procedure, deuterium is introduced into the high pressure volume (HPV) to a pressure of 25 mbar. The deuterium permeates through the sample with the permeation flux density of $J/(N_A\,A)$, where J is the permeation flux, N_A the Avogadro constant, and A the area that is permeated by the flux. After the deuterium permeation signal is stabilized in the low pressure volume (LPV), the deuterium pressure in the HPV is increased stepwise to constant pressures of 50, 100, 200, 400, and 800 mbar. The setup is enabled to continuously run measurements for more than 25 h during automatized pressure depended measurements. The pressure measurement sequence is repeated at constant sample temperatures in the following cycle: 300 °C, 400 °C, 500 °C, and 550 °C (↑-measurement) and then back to the same temperatures until 300 °C (↓-measurement).

2.4 Data analysis of the limited regime, the activation energy, and the permeation reduction factor

The permeation process is either dominated by surface effects (surface limited regime) or by diffusion (diffusion limited regime). In case of the surface limited regime, the permeation flux J is linearly increasing with the driving pressure in the HPV p: $J = k_{r/a}\,K^2\,p$ where k_r is the recombination and k_a the adsorption rate constant. K is the solubiluty [4]. In this equation the exponent of the pressure is 1. In the case of the diffusion limited regime the permeation flux is increasing with the pressure and decreasing with the sample thickness t as follows:

$$J \;=\; \frac{D\,K}{t}\sqrt{p} \tag{1}$$

where D is the diffusivity and K is the solubility. The equation illustrates that the exponent of the pressure is $n = 1/2$ [15, 17]. In this diffusion limited case, the temperature dependence on the permeation flux can be expressed by [15, 33]:

$$J = \tfrac{D_0\,K_0}{t}\sqrt{p}\cdot\exp(-E_\mathrm{P}/RT) \tag{2}$$

where R is the ideal gas constant, T is the temperature, D_0 is the diffusion constant, and K_0 is the solubility constant. The permeation activation energy E_P is defined by $E_\mathrm{P} = E_\mathrm{D} + E_\mathrm{s}$ with the activation energies of the diffusion E_D and of the solubility E_s. The evaluation of the permeation constant $P_0 = D_0K_0$ from the measurement data is introduced in [1].

The permeation barrier performance is expressed by the Permeation Reduction Factor (PRF) that is the ratio of the permeation fluxes through the bare substrate and through the coated substrate: $f_\mathrm{PRF} = J_\mathrm{bare}/J_\mathrm{coated}$.

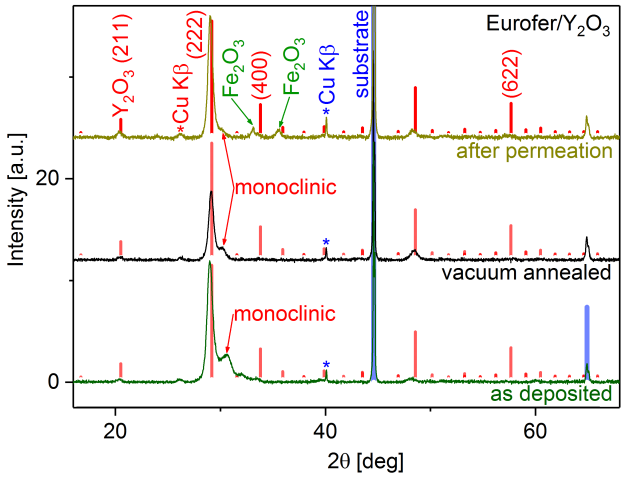

Fig. 1: Diffraction patterns after background subtraction of an Eurofer/yttria sample as deposited, after the annealing in vacuum, and after the permeation measurement. The peak intensity of the monoclinic phase decreases with the annealing time.

3 Results and discussion

3.1 Crystallographic phase and microstructure

Figure 1 shows the diffraction patterns of the Eurofer/yttria samples in three different annealing conditions: without annealing; after the annealing for 15 h at 550 °C in vacuum; and after the annealing and the permeation measurements. The literature peak positions and intensities of the Y_2O_3 cubic phase are depicted by the bars in red. The peaks of the Eurofer substrate are visible, represented by the corresponding literature bars in blue. The XRD analysis result of the lattice constant of the yttria after annealing is $a = 10.617(5)$ Å. The lattice constant is reduced during annealing and converges to its literature value [16]. The reflexes show that after annealing the yttria thin films crystallize in the cubic phase structure, which contains a small amount of a monoclinic phase. This monoclinic phase is decreasing with the annealing time, demonstrated by the marked "monoclinic" reflexes in figure 1. The long annealing time between 300 °C and 550 °C for 20 days during the permeation measurement cycles nearly eliminates the monoclinic phase, shown by the decreasing monoclinic reflex intensity with annealing time. Several identically manufactured yttria thin films confirm this phase change with the annealing time. The two low intensity iron oxide (Fe_2O_3) reflexes in figure 1 indicate the formation of iron oxide at the interlayer during the permeation measurements. The iron atoms stem from the Eurofer substrate. The formation of metal oxide islands at the interface with a maximum thickness of 20 nm is confirmed by SEM cross section images after the permeation measurements (not shown). However, the possible increase of the permeation reduction factor due to metal oxide interlayers is negligible in the following permeation measurements of this work. This is shown by the observation of smaller total permeation reduction factors of $Y_2O_3\backslash Fe_2O_3\backslash$Eurofer systems with different Y_2O_3 grain structures and with approximately 50 nm thick iron oxide interlayers [4, 16].

Figure 2 illustrates that the annealing does not lead to crack formation or delamination of the palladium layer on the yttria thin film. The same is valid for the palladium layer on the Eurofer substrates [4]. Consequently, these samples are suitable for the permeation measurements.

In [16] the thermomechanical stability, the columnar grain structure, and the Y_2O_3 stoichiometry of these yttria thin films are verified.

3.2 Stabilization time of the permeation measurements

In advance of the measurements, there is no deuterium dissolved in the samples. As the deuterium reaches the material surfaces during the permeation measurements, the yttria, the palladium, and the Eurofer are filled by the deuterium. The deuterium filling of the yttria thin film takes some hours under the deuterium pressures in

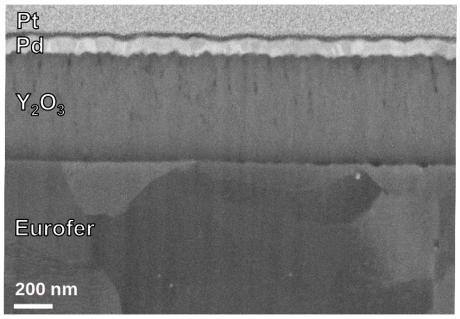

Fig. 2: SEM image (SE) of the cross section of an Eurofer/yttria/palladium sample after annealing. The Pt is there to protect the sample surface from the Ga ion beam (FIB).

the measurements since the diffusion processes in the thin films are slow. The thin film has to be refilled at each temperature level of the measurements since the yttria thin films desorb the deuterium to the vacuum of the permeation setup over 300 °C. The holding times of Eurofer/yttria of 30 min at each constant pressure level are too short to complete the deuterium filling process. Consequently, the permeation flux does not reach a constant value for the pressure levels below 400 mbar, as shown in the diagram of the measurement signals of the permeation flux over the measurement time in figure 3.

This short stabilization time strongly influences the pressure dependent analysis results of the exponent n of the limiting regime. Due to this influence, the regime not necessarily correlates with the identified exponent of the measurements with the short stabilization times of 30 min and in those measurements, the regime can not be identified [16]. However, the influence of this short stabilization time on the measurement results of the PRF is negligible, due to the stabilized permeation flux at 800 mbar. Thus, the result of the PRF is valid and based on a stabilized permeation flux measurement.

In order to stabilize the permeation flux, in this study the holding time at each pressure level is prolonged from 30 min (figure 3) to 180 min in the measurements of Eurofer/yttria/palladium (figure 4). The diagram in figure 4 shows that this longer holding time is sufficient for the deuterium flux stabilization.

In the evaluation of all samples, it is taken into account that the permeated deuterium atoms form D_2 and HD molecules. The hydrogen in the HD molecule stems from hydrogen impurities in the LPV. In case of a low D_2 signal and a large H_2 background signal, the HD signal is not negligible. This is only the case in the measurements of Eurofer/yttria/palladium, as shown in figure 4.

3.3 Permeation reduction factor and limiting regime

The remarkably high hydrogen permeation through palladium is widely reported in literature [34, 15, 35]. It is confirmed by the permeation measurement results in this study. Figure 5 shows the double logarithmic plot of the permeation flux density and the pressure in the HPV. The 500 °C↓-curves of the permeation measurements of the bare Eurofer sample and of the palladium coated Eurofer sample (Eurofer/palladium) are plotted in the upper part of this diagram. These two measurement curves show nearly the same permeation flux densities and slopes that confirm that the palladium coating nearly not reduces the permeation flux. The very slightly lower permeation flux through Eurofer/palladium might be caused by an insignificant ratio of the palladium thin film that is oxidized to PdO [4]. The hydrogen permeates the bare Eurofer as well as the Eurofer/palladium in the diffusion limited regime that is shown by the exponent of $n = 1/2$ of these two curves.

Each ↑-measurement curve of the bare Eurofer and of the Eurofer/palladium system matches the corresponding ↓-measurement curve [4]. This shows that the permeation flux at each temperature remains stable within the 7 measurement days, indicating that in the measurement a further surface oxidation of the Eurofer does not occur.

In this study all coated Eurofer substrates have identically manufactured Y_2O_3 thin films on both sides. The 550 °C and the 500 °C↓ permeation measurement curves of Eurofer/yttria/palladium are shown in figure 5. The

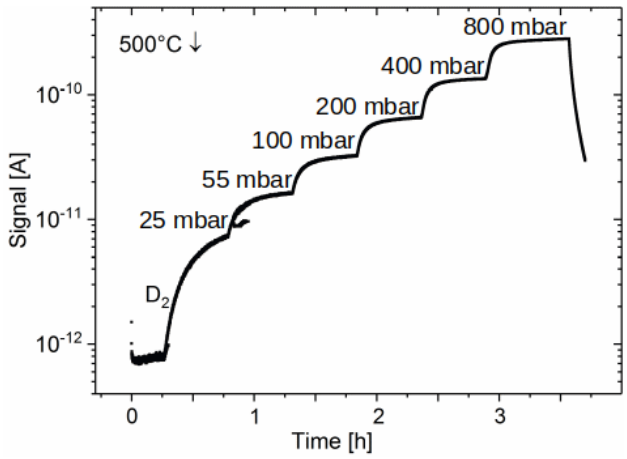

Fig. 3: Signal at 4 amu/q of the quadrupole mass analyzer over the measurement time of an Eurofer/yttria sample at 500 °C↓. The holding time of each pressure step between 25 mbar and 800 mbar is 30 min.

exponent of the exponential fit to the two curves is $n = 0.5 \pm 0.1$, demonstrating that hydrogen permeates in the diffusion limited regime. In all these experiments the deuterium flux is sufficiently stabilized for the identification of the limiting regime (section 3.2). In the measurements with a stabilization time of 180 min and in further measurements with even longer stabilization times the observed exponent n shows consistently the same value of 0.5 [4].

The thickness dependence of the permeation flux is measured with a sample with a both-sided yttria thin film thickness of 360 nm ("thin sample") [4]. All 500 °C↓ measurement results are shown in the bar chart in figure 6. After 15 h pre-annealing time the thin sample and the sample with the standard film thickness of 1020 nm show the same PRF per thickness. This demonstrates the thickness dependence of the diffusion limited regime (equation 1). Consequently, this result also confirms the permeation in the diffusion limited regime.

Due to the above discussed large hydrogen permeation through palladium, the permeation experiment of the yttria thin films with palladium top layers enable a permeation analysis that is independent of surface effects. Thus, the surface effects at the yttria surface to the gas phase does not contribute to the PRF in this experiment. Consequently, this PRF is exclusively caused by the diffusion limiting effects in the yttria thin film or by interface effects at an interface between two materials inside the sample. At 500 °C↓ the PRF of Eurofer/yttria/palladium amounts 5000 ± 850 (figures 5 and 6). In terms of permeation reduction, this PRF is a very promising measurement result, since this laboratory experiment simulates the same diffusion limiting effects of the yttria and the same interface effects of the Eurofer/yttria interface as in the application for the first wall component in future fusion power plants. Thus, the diffusion limited regime of the yttria thin film is identified in three independent points: the results of this experiment with the palladium top layers, the pressure dependence of the permeation flux, and the thin film thickness dependence of the permeation flux.

In principle, in the case of the surface limited regime, the palladium coating increases the permeation flux through Eurofer/yttria/palladium compared to Eurofer/yttria. In the case of the diffusion limited regime, the permeation flux with and without palladium top layer should be the same. However, none of these two theoretical cases are observed in the measurements. The observed permeation flux through Eurofer/yttria/palladium is lower than through Eurofer/yttria, as illustrated in figure 6. This leads to the conclusion that another effect influences the permeation flux, as discussed in the following section.

3.4 Influence of the annealing time on the permeation flux

There are two effects that influence the permeation flux over the permeation measurement time. The first effect is the deuterium filling, which increases the permeation flux on short time scales of a few hours. The second effect decreases the permeation flux on longer time scales of several days of pre-annealing in the permeation measurement or in the oven. Thus, the second effect has no impact on the measurement of the exponent n within the short time scale of 21 h.

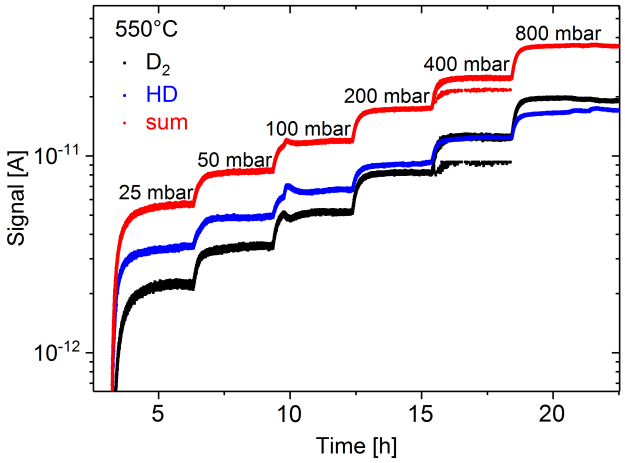

Fig. 4: Signals at 4 amu/q of the quadrupole mass analyzer over the measurement time of Eurofer/yttria/palladium at 550 °C after background subtraction. The holding time of each pressure step between 25 mbar and 800 mbar is 180 min. The different calibration coefficients of the molecules D_2 and HD are considered with a proportional factor, multiplied to the HD-curve. The sum of the D_2 and HD signals represents the signal of the total amount of the permeated D atoms.

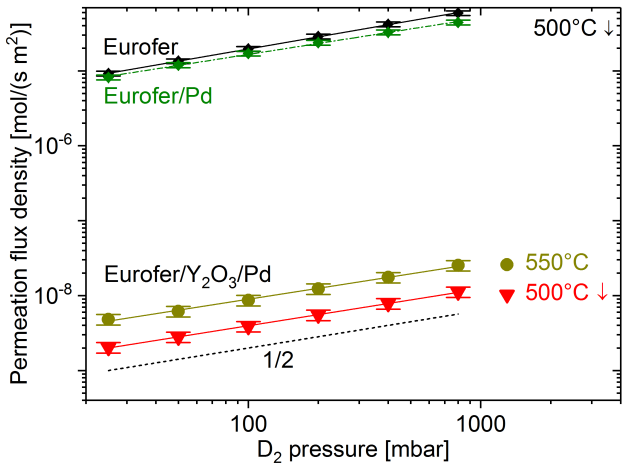

Fig. 5: Pressure dependent permeation measurement results of the pure Eurofer substrate at 500 °C↓, of a Eurofer/palladium sample at 500 °C↓, and of a Eurofer/yttria/palladium sample at 550 °C and at 500 °C↓. In this double logarithmic plot the slope of 1/2 of the fits with the exponential function equals the exponent $n = 1/2$ of the diffusion limited regime, as illustrated by the dashed 1/2-curve.

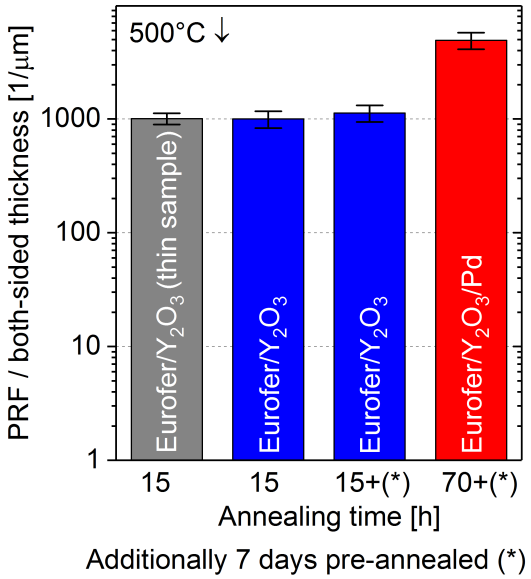

Fig. 6: Bar chart of the Permeation Reduction Factor (PRF) per both-sided Y_2O_3 coating thickness depending on the pre-annealing time. The measurement results at 500 °C↓ of the Eurofer/yttria and the Eurofer/yttria/palladium samples are shown. One of the Eurofer/yttria samples features the thinner total yttria coating thickness of 360 nm (thin sample). The total yttria coating thickness of all other standard samples is 1020 nm. Two of the samples are additionally annealed in a previous permeation measurement cycle for 7 days (*).

The bar chart in figure 6 illustrates that the hydrogen permeation reduction factor (PRF) increases with the pre-annealing time in the oven. Also, the bar chart shows the increasing PRF of Eurofer/yttria within the 7 days annealing-time between the first (15 h) and the second measurement cycle (15 h+(*)). This increase of the PRF at temperatures between 300 °C and 550 °C is much lower, compared to the increase of the PRF at the constant pre-annealing temperature of 550 °C in the oven.

Eurofer/yttria/palladium has the longest pre-annealing time for 70 h in the oven and additional 7 days in a permeation measurement cycle. It shows the largest PRF. In section 3.3 it is shown that the palladium coating cannot cause this increase of the PRF, comparing the different samples. This leads to the conclusion that the large PRF of Eurofer/yttria/palladium is a consequence of its longer pre-annealing time, compared to the other samples. The increase of the PRF with longer annealing time is observed in all experiments of all analyzed "hot metallic" yttria samples investigated in [4].

This increase of the PRF with annealing time could be induced by a crystallographic phase change from the monoclinic and cubic mixed phase of the yttria to the pure cubic phase, which is still in progress after the pre-annealing time of 15 h. In figure 1 the diffractogram illustrates that this thermally induced phase change leads continuously to the decrease of the ratio of the monoclinic phase in the yttria thin film, as discussed in section 3.1. This suggests that the monoclinic yttria phase shows higher hydrogen permeation than the cubic yttria phase. Er_2O_3 also shows a higher permation flux through its monoclinic phase than through its cubic phase [36]. The similar structure of Y_2O_3 and Er_2O_3 might lead to this similarity in the permeation characteristics. In the diffraction patterns in figure 1 the low intensities of the reflex in the monoclinic phase indicate that only a small fraction of the grains in the barrier change their crystallographic phase. The permeation flux flows primarily through the grains with the lowest permeation reduction. Due to the columnar grain structure, this primary portion of the flux permeates the grains in the monoclinic phase and reaches the other side of the barrier as in a short circuit. Thus, the small fraction of the grains in the originally monoclinic phase could induce the large increase in the permeation reduction by a factor of 5.

3.5 Activation energy

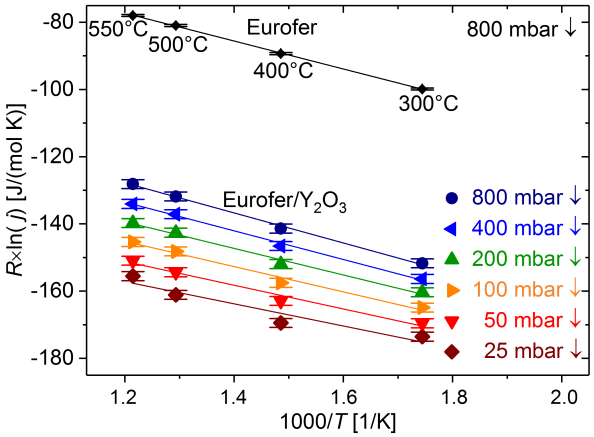

Fig. 7: Arrhenius plots of a pure Eurofer substrate at 800 mbar↓ and of Eurofer/yttria after the standard pre-annealing in oven and the additional annealing time of 7 days in the previous permeation measurement cycle at the marked pressures. The permeation flux density is expressed by the dimensionless quantity $j = J \cdot 1,882 \cdot 10^{-20}\,\mathrm{s\,m^2/mol} = J/(N_A\,A)\,\mathrm{s\,m^2/mol}$.

In this study, the permeation through all samples is purely limited by diffusion. In the following, the temperature dependent measurements of the deuterium permeation are discussed.

The permeation measurement results of pure Eurofer at the pressure of 800 mbar↓ is plotted in the upper part of each Arrhenius plot in the figures 7 and 8. In these plots the slope of the curve corresponds to the permeation activation energy. For the hydrogen permeation through the pure Eurofer it results to $E_\mathrm{P}^{(\mathrm{Eurofer})} = 41,6 \pm 0,5\,\mathrm{kJ/mol}$. This is in good agreement with the activation energy of the hydrogen permeation through the RAFM (reduced activation ferritic martensitic) steel in literature $E_\mathrm{P}^{(\mathrm{RAFM})} = E_\mathrm{D} + E_\mathrm{s} = 13,2\,\mathrm{kJ/mol} + 28,6\,\mathrm{kJ/mol} = 41,8\,\mathrm{kJ/mol}$ [15]. The permeation constant of the permeation through pure Eurofer is identified as $P_0 = 4 \cdot 10^{-8}\,\mathrm{mol/(m\,s\,\sqrt{Pa})}$ that is in very good agreement with the value in [1].

The Arrhenius plot in figure 7 shows the results of Eurofer/yttria in the pressure range between 25 mbar↓ to 800 mbar↓. The best alignment of the exponential fit is reached for the 800 mbar↓ measurement curve, due to the best permeation flux stabilization of each measurement at 800 mbar↓. In the following only the 800 mbar↓ results are discussed.

The Arrhenius plot in figure 8 shows the measurement curves at 800 mbar↓ of Eurofer/yttria and of Eurofer/yttria/palladium after the short and the long pre-annealing times, respectively. These permeation measurement results in dependence on the pre-annealing time indicate that the cubic and monoclinic mixed phase of yttria ($E_\mathrm{P}^{\text{short pre-annealed}} = 45 \pm 2\,\mathrm{kJ/mol}$) shows lower activation energy than the pure cubic phase of yttria ($E_\mathrm{P}^{\text{long pre-annealed}} = 68 \pm 2\,\mathrm{kJ/mol}$). This refers to the discussion of the crystallographic phase change with the annealing time in section 3.4.

Figure 8 illustrates an inversely proportional relation between the activation energy and the hydrogen permeation flux through yttria, since the largest activation energy (largest slope) belongs to the sample with the lowest permeation flux. This is supported by more measurement results shown in [4]. Referring to the different yttria films in this study, the evaluation of the activation energy E_P and of the permeation constant P_0 indicate that the activation energy dominantly effects the permeation flux J through the yttria films (equation 2), as shown in [4]. This indicates that the activation energy is the dominant physical property that causes the larger permeation reduction factor of the yttria in the pure cubic phase, compared to the mixed phase.

4 Conclusions

Yttria thin films after a pre-annealing time of 70 h at 550 °C show a permeation reduction factor of 5000 ± 850. The diffusion limited regime of the yttria thin film is identified in three points: the pressure dependence of the permeation flux, the thin film thickness dependence of the permeation flux, and the results of a permeation experiment of a sandwich yttria thin film with the palladium top layer.

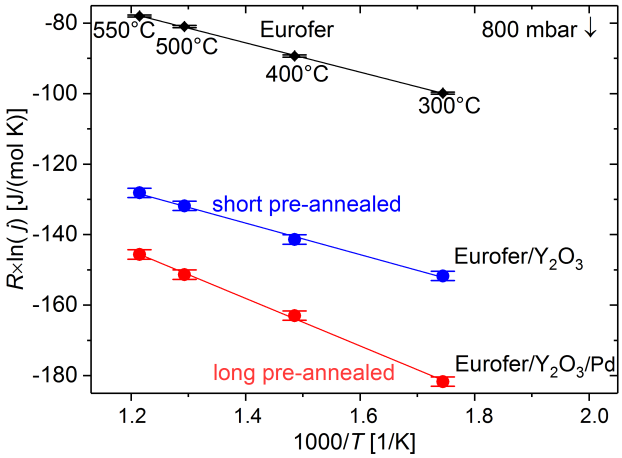

Fig. 8: Arrhenius plots at 800 mbar↓ of a pure Eurofer substrate, Eurofer/yttria, and Eurofer/yttria/palladium. The permeation flux density is expressed by the dimensionless quantity $j = J \cdot 1,882 \cdot 10^{-20}\,\mathrm{s\,m^2/mol} = J/(N_A\,A)\,\mathrm{s\,m^2/mol}$.

After the standard pre-annealing at 550 °C for 15 h the yttria thin films show a Y_2O_3 stoichiometry. The pre-annealed yttria thin films show the crystallographic cubic phase with a small fraction of the monoclinic phase. The fraction of the monoclinic phase decreases with longer annealing times and is nearly eliminated in the annealing during the permeation measurements. The permeation measurements demonstrate that this phase change causes an increase in the permeation reduction factor by a factor of 5 for extended annealing times, such as 70 h at 550 °C. This suggests that the yttria monoclinic phase shows a higher hydrogen permeation than the cubic phase. The temperature dependent permeation measurements indicate that the activation energy for permeation is lower for the cubic and monoclinic mixed phase of the yttria ($45 \pm 2\,\mathrm{kJ/mol}$), compared to the pure cubic phase of the yttria ($68 \pm 2\,\mathrm{kJ/mol}$).

These permeation measurements over long time scales of more than two weeks show that the permeation reduction factor of the yttria barrier layers is sufficiently large for applications in fusion energy technologies.

Acknowledgment

The authors gratefully thank M. Rasinski for providing FIB/SEM images and B. Göths for the polishing of the samples.

This work has been carried out within the framework of the EUROfusion consortium and has received funding from the Euratom research and training programme 2014-2018 and 2019-2020 under grant agreement No 633053. The views and opinions expressed herein do not necessarily reflect those of the European Commission.

References

[1] Houben, A., Engels, J., Rasiński, M. & Linsmeier, C. Comparison of the hydrogen permeation through fusion relevant steels and the influence of oxidized and rough surfaces. *Nuclear Materials and Energy* **19**, 55–58 (2019).

[2] Serra, E., Benamati, G. & Ogorodnikova, O. Hydrogen isotopes transport parameters in fusion reactor materials. *Journal of Nuclear Materials* **255**, 105 – 115 (1998).

[3] Byeon, W., Lee, S. & Noh, S. Transport of hydrogen and deuterium in 316LN stainless steel over a wide temperature range for nuclear hydrogen and nuclear fusion applications. *International Journal of Hydrogen Energy* **45**, 8827–8832 (2020).

[4] Engels, J. *Yttriumoxid-Dünnschichten als Tritium-Permeationsbarriere.* Ph.D. thesis, Ruhr-Universität Bochum. Available at http://d-nb.info/1177364441 (2018).

[5] Franza, F. Tritium transport analysis in HCPB DEMO blanket with the FUS-TPC code. *Fusion Engineering and Design* **88**, 2444–2447 (2013).

[6] Nakamura, H. Case study on tritium inventory in the fusion DEMO plant at JAERI. *Fusion Engineering and Design* **81**, 1339 – 1345 (2006).

[7] Reiter, F. Solubility and diffusivity of hydrogen isotopes in liquid $Pb_{17}Li$. *Fusion Engineering and Design* **14**, 207–211 (1991).

[8] Aiello, A., Ciampichetti, A. & Benamati, G. Determination of hydrogen solubility in lead lithium using sole device. *Fusion Engineering and Design* **81**, 639–644 (2006).

[9] Levchuk, D., Levchuk, S., Maier, H., Bolt, H. & Suzuki, A. Erbium oxide as a new promising tritium permeation barrier. *Journal of Nuclear Materials* **367**, 1033 – 1037 (2007).

[10] Chikada, T. *et al.* Deuterium permeation behavior of erbium oxide coating on austenitic, ferritic, and ferritic/martensitic steels. *Fusion Engineering and Design* **84**, 590–592 (2009).

[11] Zhu, J. *et al.* Growth and characterization of yttrium oxide films by reactive magnetron sputtering. *Thin Solid Films* **519**, 4894–4898 (2011).

[12] Wang, L., Pan, Y., Ding, Y. *et al.* High-pressure induced phase transitions of Y_2O_3 and Y_2O_3: Eu^{3+}. *Applied Physics Letters* **94**, 061921 (2009).

[13] Hollenberg, G., Simonen, E., Kalinin, G. & Terlain, A. Tritium/hydrogen barrier development. *Fusion Engineering and Design* **28**, 190 – 208 (1995).

[14] Perujo, A. & Forcey, K. Tritium permeation barriers for fusion technology. *Fusion Engineering and Design* **28**, 252 – 257 (1995).

[15] Causey, R., Karnesky, R. & San-Marchi, C. Tritium barriers and tritium diffusion in fusion reactors. *Comprehensive Nuclear Materials, Elsevier* 511 – 549 (2012).

[16] Engels, J., Houben, A., Hansen, P., Rasinski, M. & Linsmeier, C. Influence of the grain structure of yttria thin films on the hydrogen isotope permeation. *International Journal of Hydrogen Energy* **43**, 22976–22985 (2018).

[17] Engels, J., Houben, A., Rasinski, M. & Linsmeier, C. Hydrogen saturation and permeation barrier performance of yttrium oxide coatings. *Fusion Engineering and Design* **124**, 1140–1143 (2017).

[18] Chikada, T., Tanaka, T., Yuyama, K. *et al.* Crystallization and deuterium permeation behaviors of yttrium oxide coating prepared by metal organic decomposition. *Nuclear Materials and Energy* **0**, 1 – 6 (2016).

[19] Wu, Y., Jiang, L. & He, D. Effect of Cr_2O_3 layer on the deuterium permeation properties of Y_2O_3/Cr_2O_3 composite coating prepared by mocvd. *International Journal of Hydrogen Energy* **41**, 16101–16107 (2016).

[20] Wu, Y., He, D. & Zhang, H. Preparation of yttrium oxide coating by MOCVD as tritium permeation barrier. *Fusion Engineering and Design* **90**, 105–109 (2015).

[21] Wu, Y. *et al.* Influence of annealing atmosphere on the deuterium permeation of Y_2O_3 coatings. *International Journal of Hydrogen Energy* **41**, 10374–10379 (2016).

[22] Lei, P., Zhu, J., Zhu, Y., Jiang, C. & Yin, X. Yttrium oxide thin films prepared under different oxygen-content atmospheres: microstructure and optical properties. *Applied Physics A* **108**, 621–628 (2012).

[23] Forrest, RA and Tabasso, A and Danani, C and Jakhar, S and Shaw, AK. Handbook of activation data calculated using EASY-2007. *UKAEA FUS* **552**, 399 (2009).

[24] Nakamichi, M., Kulsartov, T., Hayashi, K., Afanasyev, S. *et al.* In-pile tritium permeation through F82H steel with and without a ceramic coating of Cr_2O_3-SiO_2 including $CrPO_4$. *Fusion engineering and design* **82**, 2246–2251 (2007).

[25] Bolatkhan, K., Kossalbayev, B. D., Zayadan, B. K., Allakhverdiev, S. I. *et al.* Hydrogen production from phototrophic microorganisms: reality and perspectives. *International Journal of Hydrogen Energy* **44**, 5799–5811 (2019).

[26] Sundarrajan, S., Allakhverdiev, S. I. & Ramakrishna, S. Progress and perspectives in micro direct methanol fuel cell. *International Journal of Hydrogen Energy* **37**, 8765–8786 (2012).

[27] Hughes, L. A., Somerday, B. P., Balch, D. K. & San Marchi, C. Hydrogen compatibility of austenitic stainless steel tubing and orbital tube welds. *International Journal of Hydrogen Energy* **39**, 20585–20590 (2014).

[28] Jones, R. H. & Thomas, G. J. Materials for the hydrogen economy. *CRC Press* (2007).

[29] Materna-Morris, E., Adelhelm, C., Baumgärtner, S. *et al.* Structural material EUROFER97. Tech. Rep., Forschungszentrum Karlsruhe (2007). Final Report on the EFDA Task.

[30] Mao, Y., Engels, J., Houben, A. *et al.* The influence of annealing on yttrium oxide thin film deposited by reactive magnetron sputtering: process and microstructure. *Nuclear Materials and Energy* **10**, 1–8 (2017).

[31] Basuki, W. & Aktaa, J. Diffusion bonding between W and EUROFER97 using V interlayer. *Journal of Nuclear Materials* **429**, 335–340 (2012).

[32] Curtis, C. Properties of yttrium oxide ceramics. *Journal of the American Ceramic Society* **40**, 274–278 (1957).

[33] Linsmeier, C., Rieth, M., Aktaa, J. *et al.* Development of advanced high heat flux and plasma-facing materials. *Nuclear Fusion* **57**, 092007 (2017).

[34] Zhang, K., Wei, X., Rui, Z., Li, Y. & Lin, Y. Effect of metal-support interface on hydrogen permeation through palladium membranes. *The American Institute of Chemical Engineers* **55**, 630–639 (2009).

[35] Wedig, F. & Jung, P. Effects of irradiation and implantation on permeation and diffusion of hydrogen isotopes in iron and martensitic stainless steel. *Journal of nuclear materials* **245**, 138–146 (1997).

[36] Chikada, T., Suzuki, A. & Kobayashi, T. Microstructure change and deuterium permeation behavior of erbium oxide coating. *Journal of Nuclear Materials* **417**, 1241 – 1244 (2011). Proceedings of ICFRM-14.